Hindawi
Advances in Materials Science and Engineering
Volume 2022, Article ID 7983231, 14 pages
https://doi.org/10.1155/2022/7983231

Research Article

The Transformation and Leachability of Fly Ash/Cement Waste Forms Subjected to the Simultaneous Effect of Heat and Chemistry

Zhao Zheng[1,2], **Hua Wen**[1,2], **Yuxiang Li**[3], **Min Qin**[1,2] **and Yao Wang**[1,2]

[1]*Shock and Vibration of Engineering Materials and Structures Key Laboratory of Sichuan Province, Southwest University of Science and Technology, Mianyang 621010, China*
[2]*School of Civil Engineering and Architecture, Southwest University of Science and Technology, Mianyang 621010, China*
[3]*School of Materials Science and Engineering, Southwest University of Science and Technology, Mianyang 621010, China*

Correspondence should be addressed to Hua Wen; 47702099@qq.com

Received 3 September 2022; Revised 22 September 2022; Accepted 28 September 2022; Published 12 October 2022

Academic Editor: Shengwen Tang

The utilization of cement waste forms with high content of fly ash is a potential method in large-volume immobilization of low- and intermedium-level radioactive waste at near-surface. However, the migration behavior of radionuclides in fly ash/cement waste forms under geological environment is still unclear. This study researched the transformation of products, pore structure as well as the leachability of Ca^{2+}, Na^{+}, and simulated radioactive nuclides (Sr^{2+} and Cs^{+}) in fly ash/cement waste forms under simultaneous effect through X-ray diffractometer (XRD), mercury intrusion porosimetry (MIP), and inductively coupled plasma optical emission spectroscopy (ICP-OES). Furthermore, the relationship between the decalcification and the leaching of Sr^{2+} and Cs^{+} was established by the fitting curves of apparent diffusion coefficient. The results indicated that the products of fly ash/cement waste forms were kept stable under simultaneous effect and the pore structure has excellent resistance to temperature. The increasing salt concentrations of leachant and temperature promoted the leaching of radionuclides while the protection layer formed at 60–80°C inhibited this phenomenon. The relationship of apparent diffusion coefficient between Sr^{2+} and Ca^{2+} was quadratic nonlinear, while the relationship between Cs^{+} and Ca^{2+} showed a linear relationship. Compared to cement waste forms, fly ash/cement waste forms were more stable. In addition, the long-term retention ability of fly ash/cement waste forms to Cs^{+} was more outstanding than Sr^{2+}.

1. Introduction

According to the national 14th five-year plan of China, the country's installed nuclear power capacity in operation will reach 70 million kilowatts by 2025. A large amount of radioactive waste liquid is produced during the operation of nuclear reactors, reprocessing of spent fuel, and decommissioning of nuclear facilities. Indeed, the volume of low- and intermedium-level radioactive waste (LILRW) liquid accounts for more than 95%. The large-volume immobilization at near-surface is a preferred method as it can improve the immobilization efficiency of LILRW and simplify the process. In order to reduce the central temperature and improve the thermal stability of the large-volume waste forms, it is necessary to add mineral admixtures, such as fly ash, metakaolin, and slag with a high dosage (up to 85%). After reaction, such mineral admixtures will transform into geopolymers [1, 2]. Besides, the fly ash-based geopolymer is regarded as a new potential solidified material for LILRW due to the characteristics of environmental protection, strong acid resistance, low permeability, and drying shrinkage [3–6], especially the excellent selective absorption and retention ability on simulated nuclides [7, 8].

In despite of the multiple protective barriers placed around the large-volume waste forms, the mass and heat transfer still occurred between the waste forms and the environment after near-surface disposal under real service conditions [9]. Due to the complexity of the underground environment (thermal-hydrological-mechanical-chemical), the combined action of these factors will lead to the

degradation of the waste forms, including the dissolution and decalcification which would result in the loose pore structure and weaken the microhardness of waste forms [10–12].

Iron compounds (amorphous iron, hematite, magnetite, etc.) in geopolymer do not participate in geopolymer reaction basically [13], but these substances will dissolve in acidic solution and produce pores. Indeed, Al^{3+} has a higher solubility under acidic conditions while the solubility of Si^{4+} is higher under alkaline conditions [13]. Temuujin [14] studied and found that geopolymer has great solubility in strong acid solution and strong alkali solution. Nguyen and Škvára [15] found that the decomposition of Si–O–Si bond would stop due to the rapid leaching of Na^+ and the occurrence of neutralization reaction in HCl solution with pH = 1, while Al–O–Si bond was more stable than Si–O–Si bond in NaOH solution with high pH. Bakharev [3] studied the durability of fly ash-based geopolymer in 5% acetic acid and sulfuric acid, and found that the degradation of geopolymer was related to depolymerization, dealuminization, replacement of Na^+ and K^+, including the formation of zeolite.

Due to the harsh external environment, the degradation of the waste forms occurred and the simulated nuclides eventually accelerated to migration outside [16]. Ofer-Rozovsky et al. [17] discovered the selectivity of geopolymers to Cs^+ by leaching experiments, and the degree of selectivity was obtained by calculating the ratio of leaching rates of Na^+ and Cs^+ at different leaching periods. For the leaching characteristics of simulated nuclides, the International Atomic Energy Agency compared the apparent diffusion coefficient (ADC) with the leaching data and established the relationship between them [18]. Abdel Rahman et al. [19] conducts the mathematical analysis of leaching data in long period and found that Sr leaching in cement waste forms was the result of the combined action of first-order reaction model and diffusion mechanism. Current studies on leaching kinetics mainly focus on first-order reaction model (FRM), first-order reaction-diffusion model (FRDM), and first-order reaction-diffusion-dissolution model (FRDDIM) [20]. Sami et al. [21] used the above kinetic models to fit the leaching data and obtained a nonlinear regression relationship, which indicated that the leaching mechanism of simulated nuclide Sr in synthetic zeolite-rich cement followed the order of first-order kinetic reaction and diffusion reaction. Xu et al. [22] found that Sr and Cs followed different kinetic models in the leaching process by adding first-order reaction-dissolution model (FRDIM) and dissolution-diffusion kinetic model (DIDM) on the basis of Sami et al. [21]. Therefore, the migration of simulated nuclides from the interior of the waste forms to the external environment conforms to the dynamic characteristics and is dominated by the corresponding migration mechanism.

However, the migration behavior of radionuclides in fly ash/cement waste forms in geological environment is not clear, and the relationship between the degradation of fly ash/cement waste forms and migration of radionuclides has not been established. Especially, it is lack of the scientific evaluation method of long-term stability and safety of radionuclides in complex geological environment. Thus, this study simulated the different geological environment by changing the leaching temperatures and the concentrations of acid leaching solution. The transformation of products and pore structure as well as the leachability of main cations (Ca^{2+} and Na^+) and simulated radioactive nuclides (Sr^{2+} and Cs^+) were researched. Then, the time required for complete leaching of Sr^{2+} and Cs^+ was calculated and deduced after the curves fitting of ADC. Also, the relationship between the decalcification of fly ash/cement waste forms and the leaching of Sr^{2+} and Cs^+ was unveiled, which is contributed to the safety evaluation of radioactive nuclides under geological environment.

2. Materials and Experiments

2.1. Materials and Preparation. The low-Ca fly ash and Portland cement (P·O 42.5, China standard: GB175-2007) were used in this study. Table 1 shows the corresponding composition of oxides in the two kinds of raw powder materials, while the particle size and morphology can be seen in reference [23]. The water used in this study was ultrapure water in order to eliminate the influence of impurities on the leaching data. Meanwhile, the inorganic salts, such $NaNO_3$, NaOH, Na_2CO_3, and NaCl, are all analytically pure.

The LILRW of 300 g/L was prepared through solving the inorganic salts one by one. Table 2 shows the concentrations of the corresponding salts. The mass ratio of total salts occupied in LILRW was 25.2%.

The fly ash/cement waste forms were prepared by mixing the raw powder materials with the LILRW under the water/binder ratio of 0.4. After stirring for 5–7 min, the fresh slurry was subjected to steam curing under 90°C for 4 h. Then, the sample was demolded and continued to be cured under 90°C for 28 d.

2.2. Leaching Experiment. Leaching experiment was conducted following with the Chinese standard GBT7023-2011 [24]. The samples were fastened with nylon thread and hung in a polyethylene bottle (volume = 250 ml) with 240 ml of NH_4Cl solution. The concentration of NH_4Cl solution ranged from 0 to 5 M while the leaching temperature was between 20 and 80°C. The Cumulative Fraction Leached (CFL) of cations in fly ash/cement waste forms were calculated through the equation shown below:

$$\mathrm{CFL} = \frac{\sum a_n / A_0}{S/V}, \tag{1}$$

where a_n is the leached mass of cations in leachate at different cumulative leaching times (g), A_0 is the initial mass of cations in samples (g) before leaching, S is the surface area of the samples (cm^2), and V is the volume of the samples (cm^3). t is the cumulative leaching times and $(\Delta t)_n$ is the leaching internal (d), $(\Delta t)_n = (\Delta t)_n - (\Delta t)_{n-1}$.

The leaching period was from 1 d to 180 d. At each leaching period, the leaching solution was refreshed. The leaching solution was ultrapure water and NH_4Cl solution with different concentrations while the leaching

Table 1: The oxides composition of raw powder materials (wt. %). (Table 1 is reproduced from [23]).

Component	CaO	SiO_2	Al_2O_3	Fe_2O_3	MgO	SO_3	K_2O	Others
Cement	62.53	20.97	4.41	2.87	3.11	3.74	0.76	1.61
Fly ash	9.08	54.71	17.04	9.69	0.55	0.59	5.22	3.12

Table 2: The salts composition of LILRW (g/L). (Table 2 is reproduced from [23]).

Salt	NaOH	$NaNO_3$	$NaAlO_2$	Na_3PO_4	Na_2SO_4	Na_2CO_3	Ca $(NO_3)_2$	Mg $(NO_3)_2$	NaCl
Content	18.95	243.08	3.32	0.20	7.60	20.69	3.32	1.80	1.04

temperatures ranged from 20 to 80°C. After the leaching experiment, the samples were crushed. Some of the fragment samples were kept in alcohol directly, and the others were ground into powders after being mixed with alcohol. Before the tests, all the samples were dried at 45°C for 24 h.

2.3. Characterization. The oxides composition of fly ash and Portland cement were determined by X-ray fluorescence (Axios, PANalytical, Netherlands) after drying to constant weight. The crystalline phases of fly ash/cement waste forms were tested by X-ray diffractometer (DMAX1400, Rigaku, Japan) from 3 to 80° of 2θ at a scanning rate of 8°/min. The pore structure of fly ash/cement waste forms with a diameter between 4 and 8 mm was determined through mercury intrusion porosimetry (Micromeritic AutoPore IV9500, USA) while the intrusion pressure ranged from 0 to 33000 PSI. The concentrations of leached cations in the leaching solution were detected through the inductively coupled plasma optical emission spectroscopy (iCP-OES 7000, Thermo Fisher Scientific, USA). Before the testing, the concentrations of Cs^+ in leaching solution were diluted into 0–10 ppm and KCl was added in the leaching solution as a shielding agent for ionization. The concentrations of Sr^{2+} and other cations were diluted into 0–30 ppm. Indeed, the pH of all the leaching solution was adjusted to about 7.

3. Results and Discussion

3.1. Transformation of Products and Pore Structures. It can be seen from Figure 1(a) that the main crystal phase in the cement waste forms of simulated LILRW is not different from the waste forms with pure $NaNO_3$ solution in previous study [24], and the crystalline phases are $Ca(OH)_2$, $CaCO_3$, and $NaNO_3$ as well as the residual C_2S. As in the simulated LILRW, the main component is still $NaNO_3$. Indeed, the content of other sodium salts is rather low, which does not appear in the XRD pattern and does not affect the types of crystal products phase in the cement waste forms. As seen from Figure 1(b), the main crystal phase obtained from the fly ash/cement waste forms mixed with simulated LILRW is not different from the waste forms with pure $NaNO_3$ solution under low content of NaOH in previous study [23]. The main crystal phase is mainly silica, mullite, and $NaNO_3$. However, under the condition of high NaOH, the phase was slightly different from the waste forms with $NaNO_3$ solution, and only the chabazite phase was generated but there was no Na–P1 zeolite which existed in the condition of $NaNO_3$ solution. Combined with previous studies about the effect of NaOH contents on the product and structure of fly ash/cement waste forms and the leaching rate of simulated radionuclides [23, 25], the NaOH content in the fly ash/cement waste forms of simulated LILRW in the study below was determined to be 10%.

As seen in Figure 2, the crystalline products in the fly ash/cement waste forms of simulated LILRW did not change after leaching in ultrapure water (0 M NH_4Cl). After leaching in 0.6 M NH_4Cl solution, the diffraction peak of $NaNO_3$ disappeared in the matrices compared to Figure 1(b). After leaching in 5 M NH_4Cl solution, the diffraction peak of $NaNO_3$ also disappeared, but the diffraction peak of NH_4Cl appeared. In all the leached samples, the crystalline phase, including zeolite phases in the fly ash/cement waste forms remain unchanged under the simultaneous effect, while the main change is in the C–S–H gel which suffered the decalcification. According to previous studies, the structure and composition of cement hydration products, especially C–S–H gel, were significantly degraded under the accelerated decalcification [26–28], which resulted in the loose pore structure of waste forms and the significant increase of leaching rate of simulated radionuclides.

As seen in Figure 3 and Table 3, the median pore diameter of cement waste forms increases obviously with the increasing concentrations of leaching solution except 5 M NH_4Cl. The porosity increases firstly and then decreases with the concentration of leaching solution, and the highest value of 20.99% is obtained at the NH_4Cl concentration of 0.6 M. The median pore diameter increases with the leaching temperature ranging from 20 to 80°C while the highest porosity of 10.53% is obtained at 60°C.

As seen in Figure 4 and Table 4, the median pore diameter of fly ash/cement waste forms also increases obviously when the leaching solution ranges from ultrapure water to 3 M NH_4Cl solution, which is similar with the change of cement waste forms. The highest porosity of 20.79% is also obtained at the NH_4Cl concentration of 0.6 M and then decreases with the increasing NH_4Cl concentration. However, the median pore diameter and porosity show little change when the leaching temperature ranges from 20 to 60°C. Though the porosity of 8.35% at 80°C is the highest at different leaching temperatures, it only increased by 1% compared with that at other leaching temperatures.

Based on the above results, it can be concluded that the products of fly ash/cement waste forms are more stable than cement waste forms under simultaneous effect. Also, the degradation of pore structure of fly ash/cement waste forms

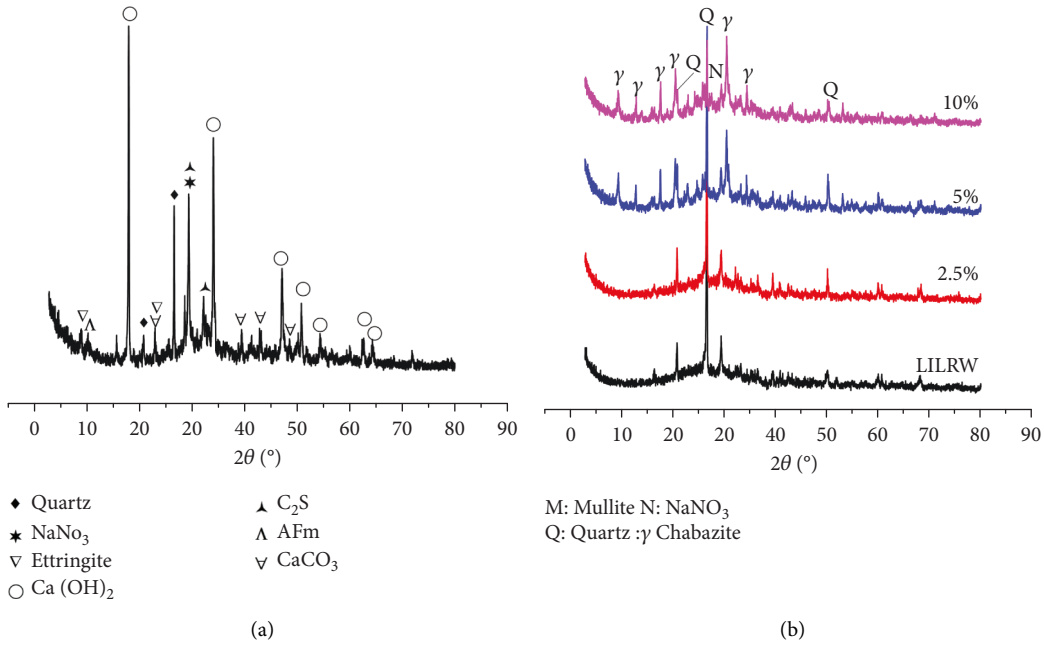

FIGURE 1: XRD patterns of waste forms of simulated LILRW: (a) cement waste forms; (b) fly ash/cement waste forms, 0.82%~10% NaOH.

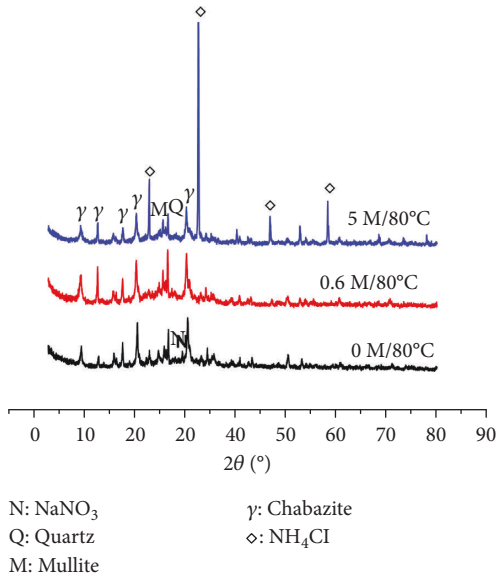

FIGURE 2: XRD patterns of fly ash/cement waste forms of simulated LILRW after leaching in different concentrations of NH_4Cl at 80°C.

is mainly caused by the decalcification of hydration products of cement [29]. Moreover, the pore structure of fly ash/cement waste forms has excellent resistance to temperature than cement waste forms as the crystalline zeolite phases does not dissolute in such moderate condition.

3.2. Leachability. Figures 5–8 show the CFL of cations in fly ash/cement waste forms under simultaneous effect. As seen in Figure 5, the CFL of Na^+ in ultrapure water is always much lower than that in NH_4Cl solution. However, with the increase of leaching temperature, the CFL of Na^+ in ultrapure water is closer to that in NH_4Cl solution. At the leaching period of 180 d, the CFL of Na^+ in ultrapure water is equivalent to that in 5 M solution at 80°C. In the early stage of leaching, the CFL of Na^+ increases while the NH_4Cl concentration ranges from 0.6 to 5 M, but decreases in the later stage. Indeed, this transition becomes earlier at the higher leaching temperature, which occurred under 14 d at 20°C and 40°C, 7 d at 60°C, and 3 d at 80°C, respectively.

As seen in Figure 6, the CFL of Ca^{2+} in ultrapure water is less than 1.5×10^{-3} cm at various leaching temperatures. At the early stage of leaching, the CFL of Ca^{2+} increases following with the rising NH_4Cl concentration. However, the CFL of Ca^{2+} in 3 M and 5 M NH_4Cl solutions is less than 0.6 M and 1 M adversely at a specific leaching period. This specific leaching period is shortened when the leaching temperature ascends, which is 154 d at 20°C, 28 d at 40°C, 63 d at 60°C, and 21 d at 80°C, respectively. With the increase of leaching temperature, the disparity of the CFL of Ca^{2+} between 3 and 5 M NH_4Cl solution and 0.6–1 M becomes more and more obvious.

The CFL of Sr^{2+} in ultrapure water is always less than 6×10^{-4} cm under various leaching temperatures, as seen in Figure 7. But the CFL of Sr^{2+} in 0.6–3 M NH_4Cl solution increases significantly following with the rising NH_4Cl concentrations, and the gap expands with the extension of leaching period. The CFL of Sr^{2+} in 5 M NH_4Cl solution was lower than that in 3 M at 20°C and higher than that in 3 M at 40 and 60°C. Nevertheless, it is significantly lower than that in 3 M at 80°C after the leaching period of 154 d.

Compared with the leaching condition of NH_4Cl solution, the CFL of Cs^+ under the condition of ultrapure water is always very low, just close to 1×10^{-5} cm, as seen in Figure 8. At each leaching temperature, the CFL of Cs^+ increases when the concentration of leaching solution rises. However, at 40°C and 80°C, the CFL of Cs^+ in 5 M and 3 M

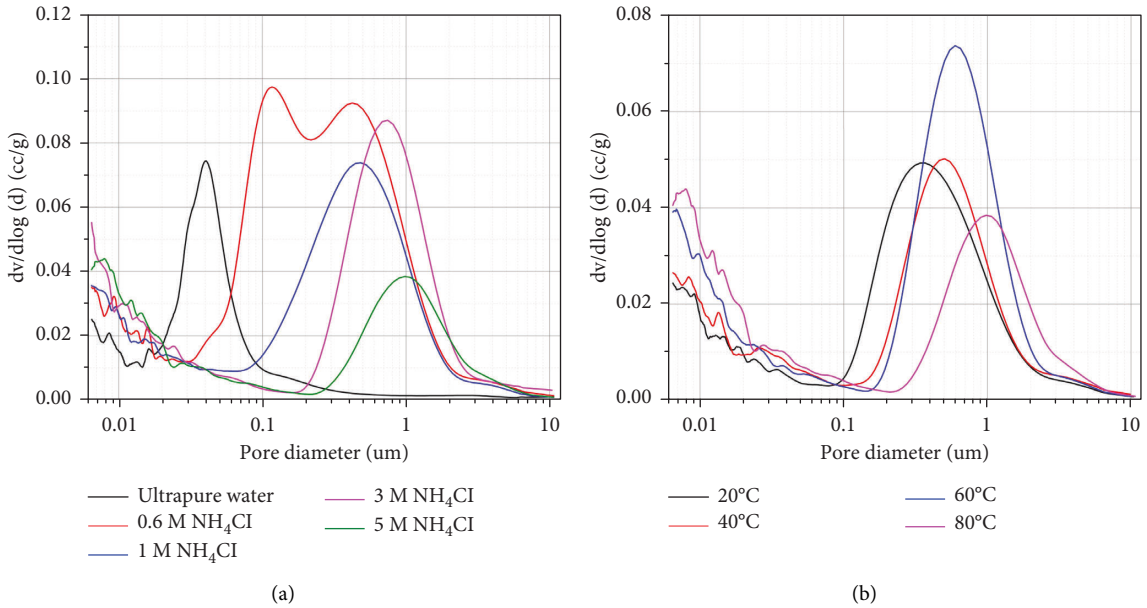

Figure 3: The distribution curves of pore diameter of cement waste forms after leaching under simultaneous effect: (a) the NH_4Cl concentration is from 0 to 5 M while the temperature is 20°C; (b) the temperature is from 20 to 80°C while the NH_4Cl concentration is 5 M.

Table 3: The characteristics of pore structure of cement waste forms.

Leaching conditions (M/°C)	0	0.6/80	1/80	3/80	5/80	5/60	5/40	5/20
Porosity (%)	7.71	20.99	13.23	11.92	7.62	10.53	8.19	9.20
Median pore diameter (nm)	39.21	232.5	374.0	621.2	526.7	503.4	426.2	339.4

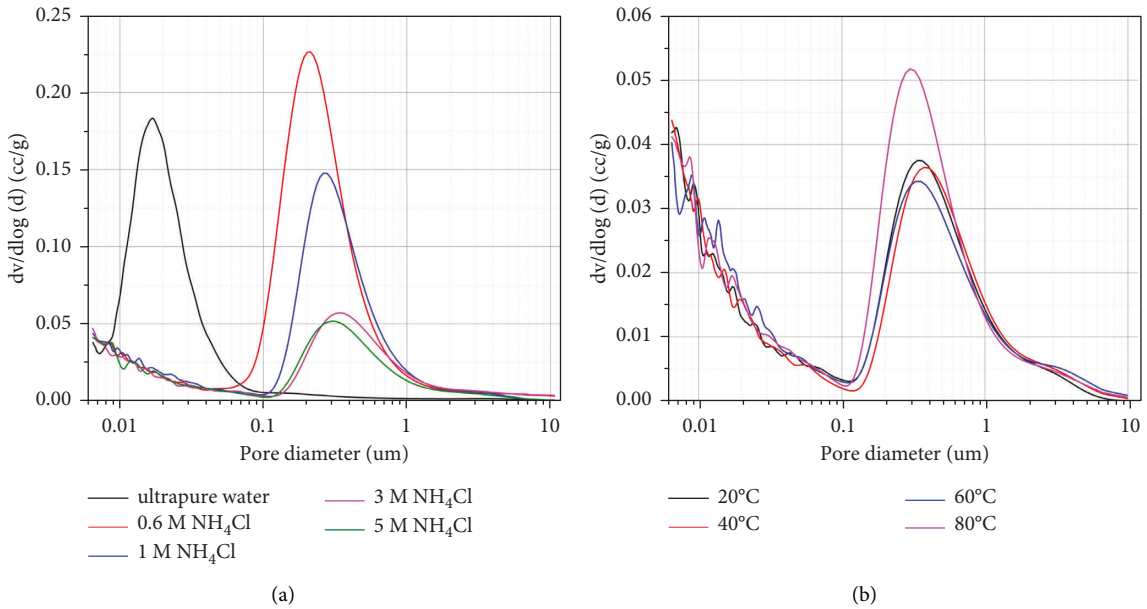

Figure 4: The distribution curves of pore diameter of fly ash/cement waste forms after leaching under simultaneous effect: (a) the NH_4Cl concentration is from 0 to 5 M while the temperature is 20°C; (b) the temperature is from 20 to 80°C while the NH_4Cl concentration is 5 M.

Table 4: The characteristics of pore structure of fly ash/cement waste forms.

Leaching conditions (M/°C)	0	0.6/80	1/80	3/80	5/80	5/60	5/40	5/20
Porosity (%)	15.52	20.79	15.31	9.05	8.35	7.20	7.21	7.45
Median pore diameter (nm)	18.67	212.3	278.2	314.0	260.5	244.2	279.3	269.3

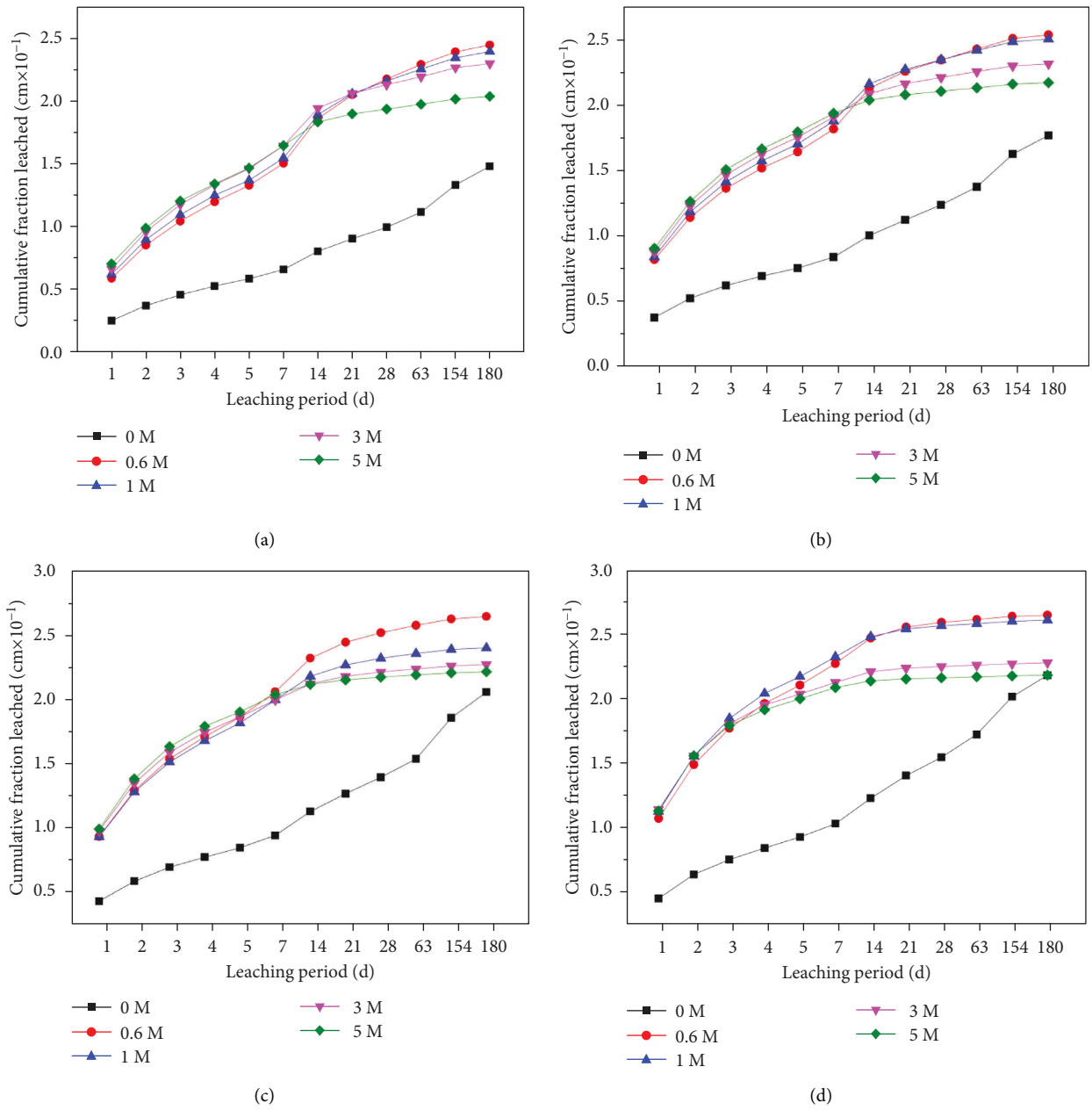

Figure 5: CFL of Na^+ in fly ash/cement waste forms under simultaneous effect: (a) 20°C; (b) 40°C; (c) 60°C; (d) 80°C.

began to be lower than that in 0.6 M at 154 d and 28 d of leaching period, respectively.

From Figures 5–8, it can be concluded that the CFL of all the cations increase with the rising temperatures and concentrations which accelerated the degradation [30]. But the leaching of cations decrease at a specific leaching period, especially at high leaching temperature of 60 and 80°C. This is mainly attributed to the crystallization of NH_4Cl at the surface and inside of fly ash/cement waste forms, which led to a dense surface to restrain the leaching of cations [31]. Also, the high NH_4Cl concentration has decreased the porosity of fly ash/cement waste forms (Figure 4 and Table 4), which contributed to the retention of radioactive nuclides. Moreover, a transition layer was formed between the inner nondegraded layer and the outer fully degraded layer [32]. The existence of transition layer was also the main factor that led to the reduction of ion leaching rate at the later stage. So, it can be concluded that the dense structure formed at the rather high temperature (60–80°C) and high NH_4Cl (3 M and 5 M) is contributed to the stability of the fly ash/cement waste forms.

3.3. Fitting of Apparent Diffusion Coefficient. The fitting process was based on the equation of Fick's second law in a semi-infinite medium, and apparent diffusion coefficient (ADC) as well as the time for complete leaching of radionuclides were calculated [21, 33, 34]. In this study, the ADC of cations in the fly ash/cement waste forms was assumed to be constant. In order to avoid the influence of the crystalline

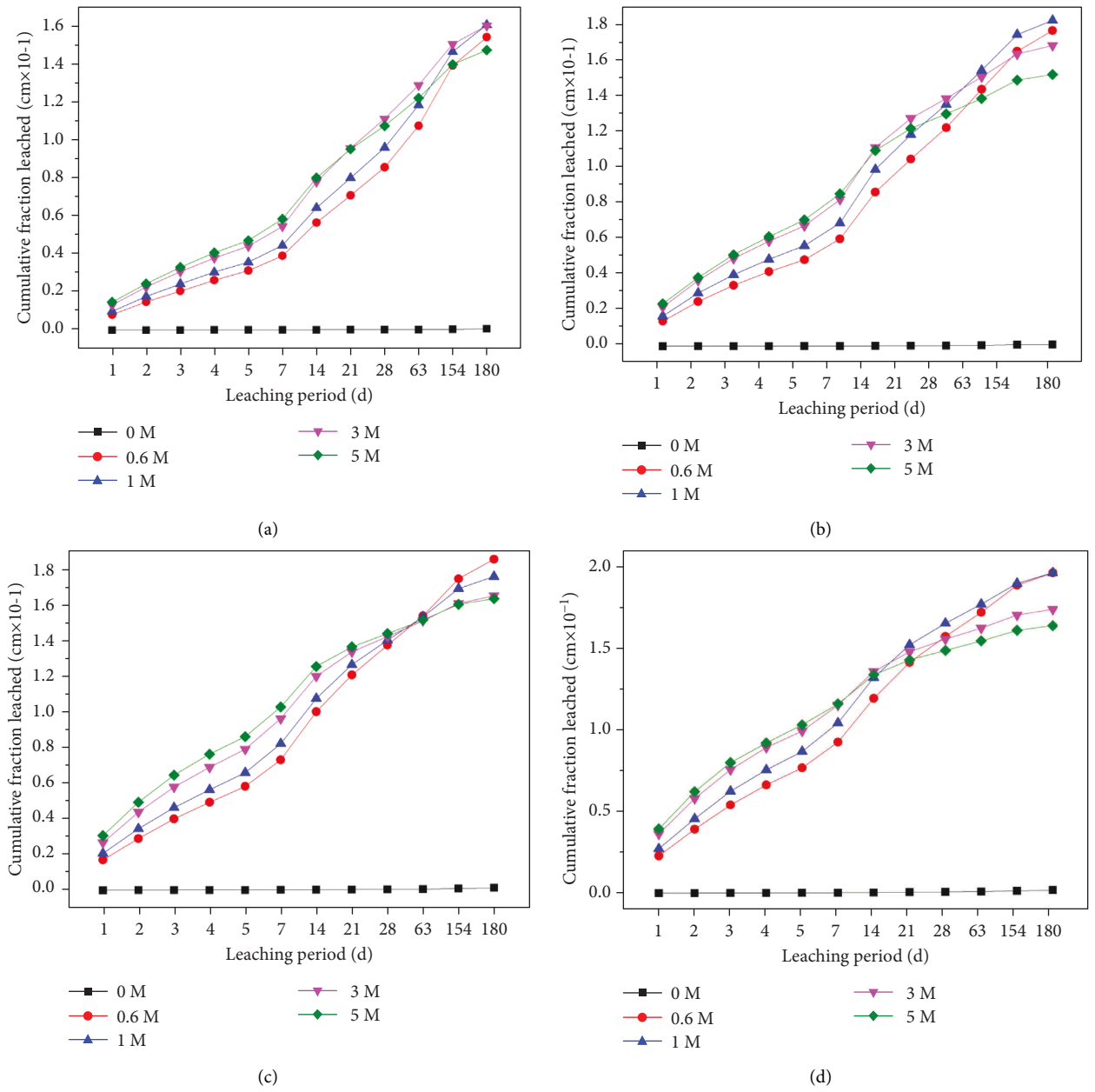

Figure 6: CFL of Ca^{2+} in fly ash/cement waste forms under simultaneous effect: (a) 20°C; (b) 40°C; (c) 60°C; (d) 80°C.

NH_4Cl on the calculation of ADC, the leaching data at the leaching period of 1–14 d were selected. As the fitting curves of other leaching temperatures of Sr^{2+} and the fitting curves of Ca^{2+} and Cs^+ are similar to Figure 9, the rest of the fitting curves are not listed one by one. Based on the phase transformation and leachability of Na^+, it can be deduced the leached Na^+ was mainly free Na^+ which has little influence on the leaching of radioactive nuclides. Thus, the fitting curves of Na^+ have not been discussed below.

After fitting, the ADC and the time for complete leaching of Sr^{2+} in the fly ash/cement waste forms are listed in Table 5. The time for complete leaching of Sr^{2+} in fly ash waste forms at ultrapure water and 20°C was the longest (2.15×10^8 d) while the shortest time was almost one month at 5 M of NH_4Cl solution and 80°C.

It can be seen from Figure 10 that both the ADC of Ca^{2+} and Sr^{2+} in fly ash/cement waste forms increase with the rising leaching temperatures and concentrations of leaching solution. As seen in Figure 11, the relationship of the ADC between Ca^{2+} and Sr^{2+} in fly ash/cement waste forms is quadratic nonlinear ($Y = 4.44 \times 10^{-5} - 0.21X + 1403.33X^2$), which is different from the linear relationship in cement waste forms [31]. When the ADC of Ca^{2+} is lower than 4×10^{-4} cm^2/d, the ADC of Sr^{2+} and Ca^{2+} can be approximately regarded as a linear relationship. However, the ADC of Sr^{2+} increases exponentially with the rising ADC of Ca^{2+} when the ADC of Ca^{2+} is above 4×10^{-4} cm^2/d.

The ADC of Cs^+ (D_{cs}) and time for complete leaching (T_{end}) are listed at Table 6. The time for complete leaching of Cs^+ in fly ash waste forms at ultrapure water and 20°C was

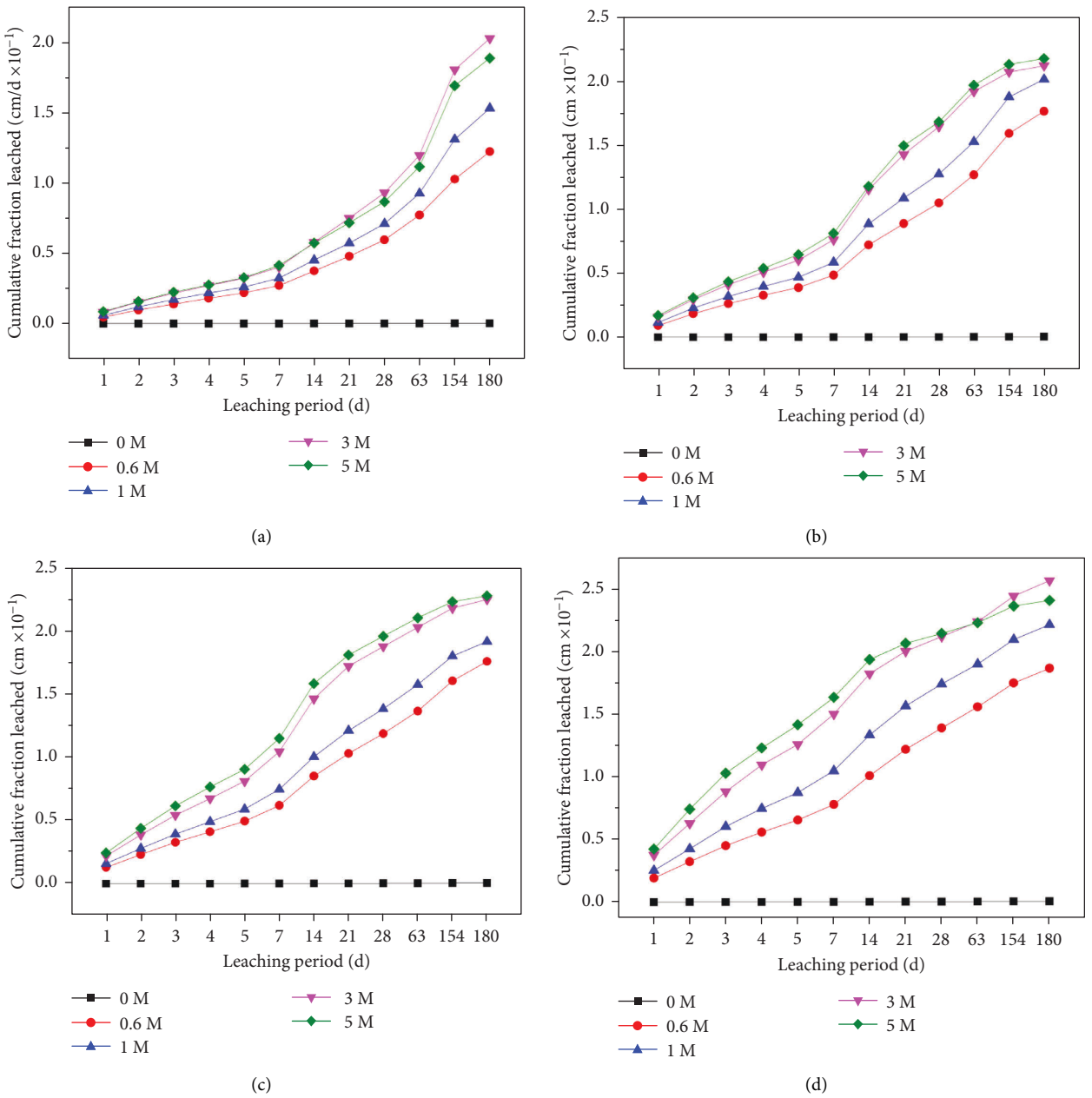

Figure 7: CFL of Sr^{2+} in fly ash/cement waste forms under simultaneous effect: (a) 20°C; (b) 40°C; (c) 60°C; (d) 80°C.

the longest (5.15×10^7 d) while the shortest time was almost two days at 5 M of NH_4Cl solution and 60°C. It can be seen from Figure 12 that the highest ADC of Cs^+ is obtained at the leaching temperature of 60°C but not the highest temperature of 80°C. This trend further indicated that the high temperature (80°C) would indeed enhance the retention ability of fly ash/cement waste forms to radioactive nuclides. Indeed, the ADC of Cs^+ increases when the concentrations of leaching solution ascend. As seen in Figure 13, the ADC of Cs^+ increases obviously with the rising ADC of Ca^{2+}, which shows a linear relationship as: $Y = -1.84 \times 10^{-10} + 6.86 \times 10^{-6} X$.

Comparing the fitting curves in Figures 11 and 13, it can be found that the leaching rate of Cs^+ was higher than Sr^{2+} at the early period of leaching experiment while it was opposite at the latter period. Due to the little ionic radius of Cs^+ and the unstable physical adsorption on zeolites [35–37], the free and adsorbed Cs^+ preferred to leach out in the solution environment all the time, which was not affected by the decalcification obviously. However, Sr^{2+} existed in fly ash/cement waste forms by chemical adsorption on C–S–H gels and partial Ca^{2+} in C–S–H gels was substituted by Sr^{2+} [38–41]. Thus, the decalcification occurred in the latter period can accelerate the leaching of Sr^{2+} sharply. Meanwhile, the decalcification led to the polymerization of C–S–H gels and the decrease of bridging oxygen, which further weakened the adsorption ability of C–S–H gels [24, 37].

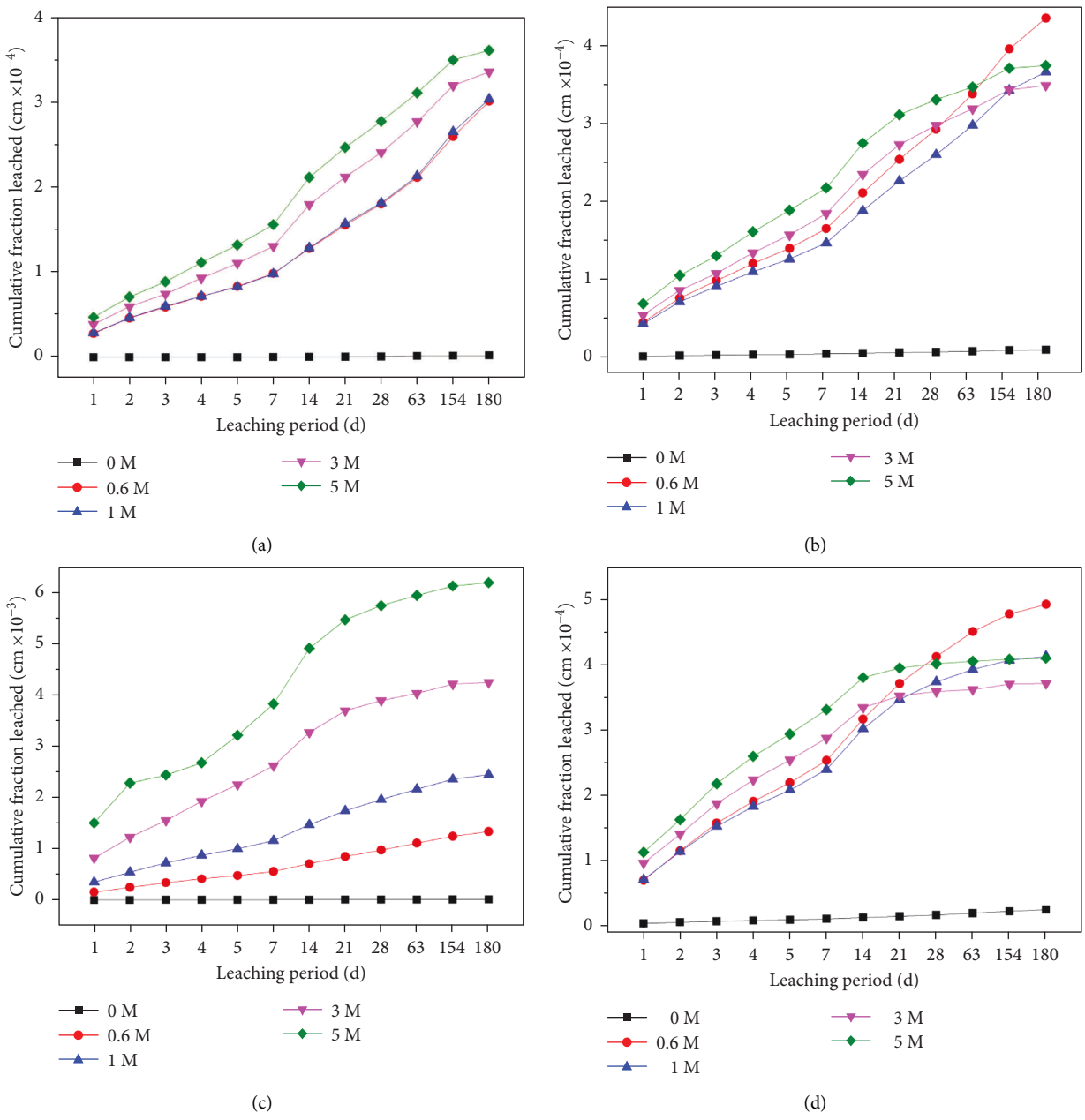

Figure 8: CFL of Cs^+ in fly ash/cement waste forms under simultaneous effect: (a) 20°C; (b) 40°C; (c) 60°C; (d) 80°C.

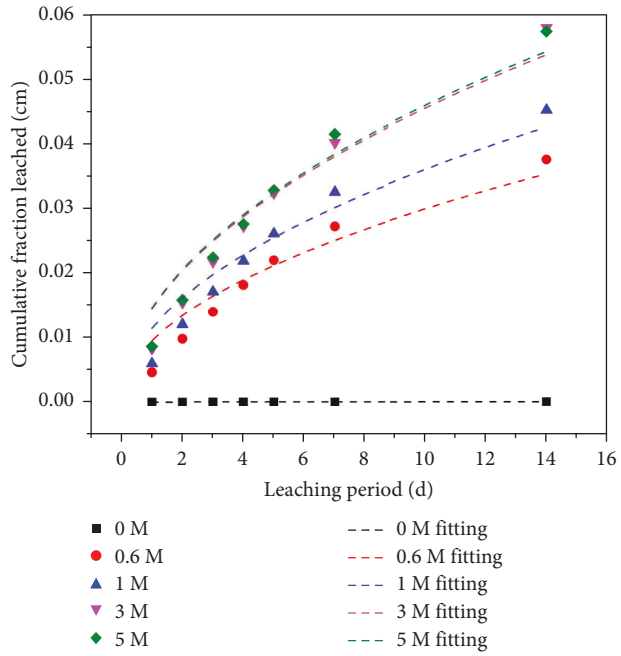

Figure 9: Fitting curve of CFL of Sr^{2+} in fly ash/cement waste forms at 20°C.

Table 5: ADC of Sr^{2+} (D_{sr}) and time for complete leaching (T_{end}).

Leaching conditions		Fly ash/cement waste forms	
		D_{sr} (cm^2/d)	T_{end} (d)
20 C	0 M	4.06×10^{-10}	2.15×10^{8}
	0.6 M	7.01×10^{-5}	1.24×10^{3}
	1 M	1.02×10^{-4}	8.58×10^{2}
	3 M	1.62×10^{-4}	5.38×10^{2}
	5 M	1.65×10^{-4}	5.28×10^{2}
40 C	0 M	1.27×10^{-9}	6.87×10^{7}
	0.6 M	2.42×10^{-4}	3.60×10^{2}
	1 M	3.60×10^{-4}	2.42×10^{2}
	3 M	6.05×10^{-4}	1.44×10^{2}
	5 M	6.53×10^{-4}	1.34×10^{2}
60 C	0 M	1.90×10^{-9}	4.58×10^{7}
	0.6 M	3.67×10^{-4}	2.37×10^{2}
	1 M	5.21×10^{-4}	1.68×10^{2}
	3 M	1.04×10^{-3}	8.38×10^{1}
	5 M	1.27×10^{-3}	6.86×10^{1}
80 C	0 M	3.78×10^{-9}	2.31×10^{7}
	0.6 M	5.87×10^{-4}	1.49×10^{2}
	1 M	1.04×10^{-3}	8.38×10^{1}
	3 M	2.09×10^{-3}	4.17×10^{1}
	5 M	2.53×10^{-3}	3.44×10^{1}

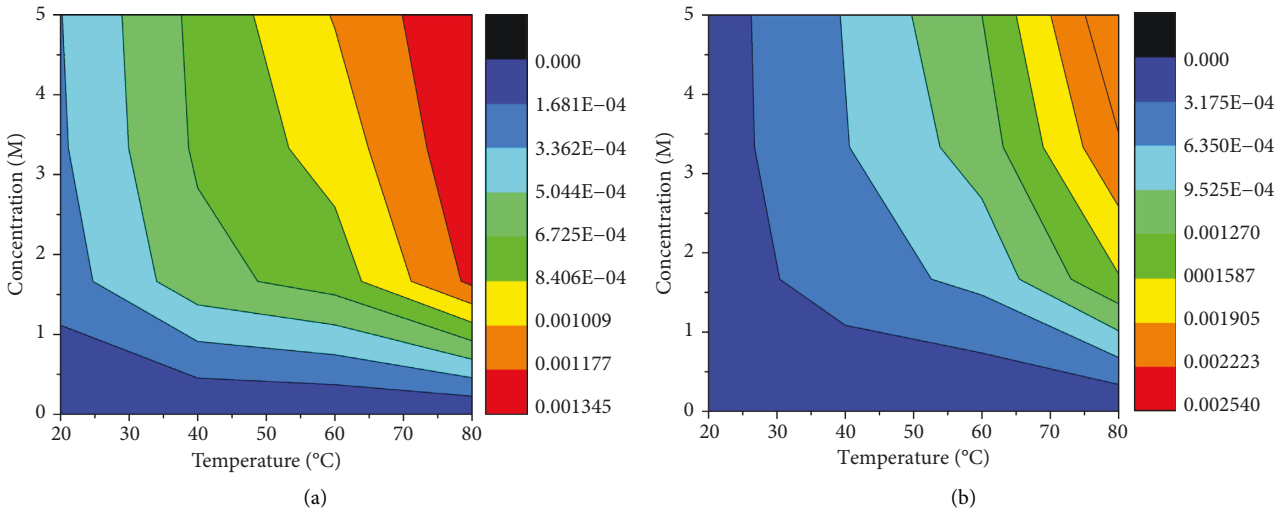

Figure 10: The distribution of ADC of Ca^{2+} and Sr^{2+} in fly ash/cement waste forms at simultaneous effect: (a) Ca^{2+}; (b) Sr^{2+}.

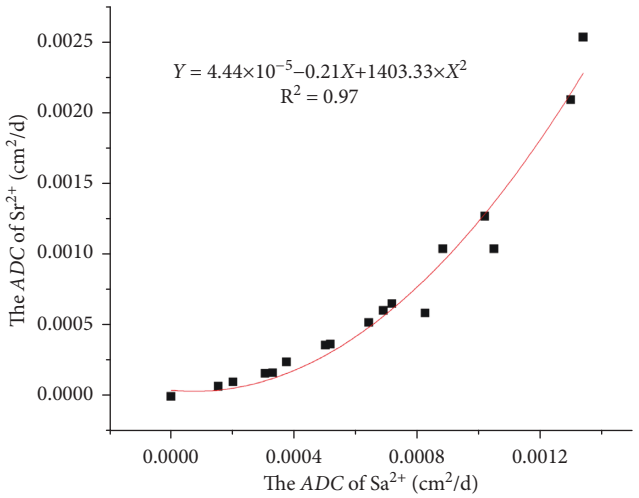

Figure 11: The relationship of ADC between Ca^{2+} and Sr^{2+} in fly ash/cement waste forms.

Table 6: ADC of Cs^{+} (D_{cs}) and time for complete leaching (T_{end}).

Leaching conditions	Fly ash/cement waste forms		
		D_{cs} (cm^2/d)	T_{end} (d)
20°C	0 M	4.64×10^{-14}	5.15×10^{7}
	0.6 M	9.78×10^{-10}	2.44×10^{3}
	1 M	9.83×10^{-10}	2.42×10^{3}
	3 M	1.77×10^{-09}	1.35×10^{3}
	5 M	2.50×10^{-09}	9.56×10^{2}
40°C	0 M	3.31×10^{-12}	7.22×10^{5}
	0.6 M	2.72×10^{-09}	8.79×10^{2}
	1 M	2.21×10^{-09}	1.08×10^{3}
	3 M	3.38×10^{-09}	7.06×10^{2}
	5 M	4.77×10^{-09}	5.00×10^{2}
60°C	0 M	5.37×10^{-12}	4.45×10^{5}
	0.6 M	3.10×10^{-08}	7.70×10^{1}
	1 M	1.35×10^{-07}	1.76×10^{1}
	3 M	6.71×10^{-07}	3.56
	5 M	1.51×10^{-06}	1.58

Table 6: Continued.

Leaching conditions		Fly ash/cement waste forms	
		D_{cs} (cm^2/d)	T_{end} (d)
80°C	0 M	1.58×10^{-11}	1.51×10^{5}
	0.6 M	6.40×10^{-09}	3.73×10^{2}
	1 M	5.85×10^{-09}	4.08×10^{2}
	3 M	8.13×10^{-09}	2.94×10^{2}
	5 M	1.08×10^{-08}	2.22×10^{2}

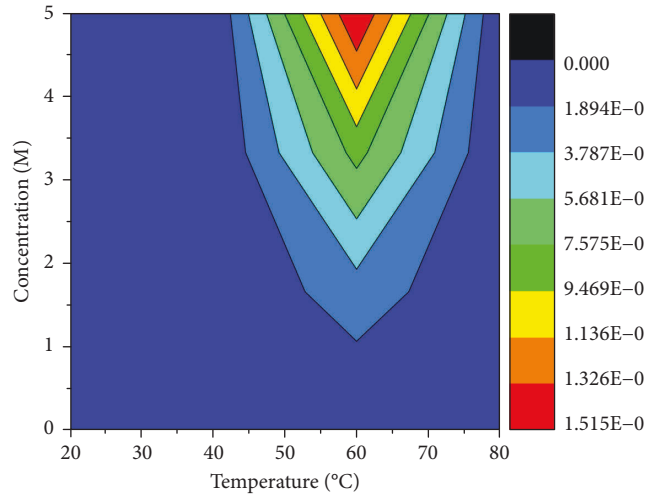

Figure 12: The distribution of ADC of Cs^+ in fly ash/cement waste forms at simultaneous effect.

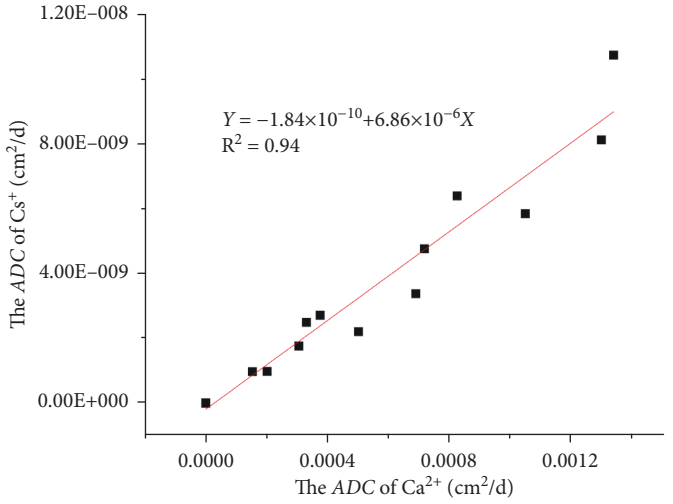

Figure 13: The relationship of ADC between Ca^{2+} and Cs^+ in fly ash/cement waste forms.

4. Conclusion

Above all, it can be concluded that the degradation of fly ash/cement waste forms was still attributed to the decalcification of the hydration products of cement. Compared to cement waste forms, fly ash/cement waste forms were more stable under simultaneous effect. Furthermore, the long-term stability of Cs^+ in fly ash/cement waste forms was better than Sr^{2+}.

(1) The products of fly ash/cement waste forms are kept stable under a simultaneous effect. The pore structure transformation of fly ash/cement waste forms under simultaneous effect were mainly attributed to the degradation of cement waste forms. Indeed, the pore structure has excellent resistance to temperature.

(2) Following with the increase of the concentrations of leaching solution and leaching temperature, all the

cations in fly ash/cement waste forms accelerated to migrate outside. But the migration of cations was restrained at a specific leaching period under high leaching temperatures (60–80°C) and NH_4Cl (3–5 M) because of the protection layer formed under these conditions.

(3) The ADC of both Cs^+ and Sr^{2+} increased with the increase of Ca^{2+}, and the relationship of ADC between Sr^{2+} and Ca^{2+} in fly ash/cement waste forms was quadratic nonlinear: $Y = 4.44 \times 10^{-5} - 0.21X + 1403.33X^2$. However, the relationship of ADC between Cs^+ and Ca^{2+} showed a linear relationship: $Y = -1.84 \times 10^{-10} + 6.86 \times 10^{-6}X$.

Data Availability

The data that support the findings of this study are available from the corresponding author upon reasonable request.

Conflicts of Interest

The authors declare that they have no conflicts of interest..

Authors' Contributions

Methodology, formal analysis, investigation, writing-original draft were performed by Zhao Zheng. Resources and supervision were performed by Hua Wen. Yuxiang Li: conceptualization and resources. Resources, formal analysis, and writing-review and editing were performed by Min Qin. Validation and resources were performed by Yao Wang.

Acknowledgments

This work was supported by the Scientific Research Fund of Southwest University of Science and Technology (No. 21zx7124). The authors gratefully acknowledge School of Civil Engineering and Architecture, School of Materials Science and Engineering (Southwest University of Science and Technology) for providing facilities to carry out the work.

References

[1] J. Davidovits, "Properties of geopolymer cements," in *First International Conference on Alkaline Cements and Concretes*Kiev State Technical University, Ukraine, 1994.

[2] J. G. S. Van Jaarsveld, J. S. J. Van Deventer, and G. C. Lukey, "The effect of composition and temperature on the properties of fly ash-and kaolinite-based geopolymers," *Chemical Engineering Journal*, vol. 89, no. 1-3, pp. 63–73, 2002.

[3] T. Bakharev, "Resistance of geopolymer materials to acid attack," *Cement and Concrete Research*, vol. 35, no. 4, pp. 658–670, 2005.

[4] K. M. Klima, K. Schollbach, H. J. H. Brouwers, and Q. L. Yu, "Thermal and fire resistance of Class F fly ash based geopolymers-A review," *Construction and Building Materials*, vol. 323, Article ID 126529, 2022.

[5] L. Wang, S. Zhou, Y. Shi et al., "The influence of fly ash dosages on the permeability, pore structure and fractal features of face slab concrete," *Fractal Fract*, vol. 6, no. 9, p. 476, 2022.

[6] L. Wang, F. X. Guo, Y. Q. Lin, H. M. Yang, and S. W. Tang, "Comparison between the effects of phosphorous slag and fly ash on the C-S-H structure, long-term hydration heat and volume deformation of cement-based materials," *Construction and Building Materials*, vol. 250, Article ID 118807, 2020.

[7] Y. Zhu, Z. Zheng, Y. Deng, C. Shi, and Z. Zhang, "Advances in immobilization of radionuclide wastes by alkali activated cement and related materials," *Cement and Concrete Composites*, vol. 126, Article ID 104377, 2022.

[8] J. F. Li, L. Chen, and J. L. Wang, "Solidification of radioactive wastes by cement-based materials," *Progress in Nuclear Energy*, vol. 141, Article ID 103957, 2021.

[9] R. Song, J. Liu, C. Yang, and S. Sun, "Study on the multiphase heat and mass transfer mechanism in the dissociation of methane hydrate in reconstructed real-shape porous sediments," *Energy*, vol. 254, no. C, Article ID 124421, 2022.

[10] F. L. Qu, W. G. Li, K. J. Wang, S. S. Zhang, and D. C. Sheng, "Performance deterioration of fly ash/slag-based geopolymer composites subjected to coupled cyclic preloading and sulfuric acid attack," *Journal of Cleaner Production*, vol. 321, Article ID 128942, 2021.

[11] M. Yang, Y. J. Zheng, X. Li, X. J. Yang, F. Rao, and L. L. Zhong, "Durability of alkali-activated materials with different C-S-H and N-A-S-H gels in acid and alkaline environment," *Journal of Materials Research and Technology*, vol. 16, pp. 619–630, 2022.

[12] L. Wang, M. Jin, S. Zhou, S. W. Tang, and X. Lu, "Investigation of microstructure of C-S-H and micro-mechanics of cement pastes under NH_4NO_3 dissolution by ^{29}Si MAS NMR and microhardness," *Measurement*, vol. 185, Article ID 110019, 2021.

[13] N. W. Chen-Tan, A. Van Riessen, C. V. Ly, and D. C. Southam, "Determining the reactivity of a fly ash for production of geopolymer," *Journal of the American Ceramic Society*, vol. 92, no. 4, pp. 881–887, 2009.

[14] J. Temuujin, A. Minjigmaa, M. Lee, N. Chen-Tan, and A. van Riessen, "Characterisation of class F fly ash geopolymer pastes immersed in acid and alkaline solutions," *Cement and Concrete Composites*, vol. 33, no. 10, pp. 1086–1091, 2011.

[15] A. D. Nguyen and F. Škvára, "The influence of ambient pH on fly ash-based geopolymer," *Cement and Concrete Composites*, vol. 72, pp. 275–283, 2016.

[16] P. G. He, J. Y. Cui, M. L. Wang et al., "Interplay between storage temperature, medium and leaching kinetics of hazardous wastes in Metakaolin-based geopolymer," *Journal of Hazardous Materials*, vol. 384, Article ID 121377, 2020.

[17] E. Ofer-Rozovsky, M. A. Haddad, G. Bar-Nes et al., "Cesium immobilization in nitrate-bearing metakaolin-based geopolymers," *Journal of Nuclear Materials*, vol. 514, pp. 247–254, 2019.

[18] A. Atkinson and A. K. Nickerson, "Diffusion and sorption of cesium, strontium, and iodine in water-saturated cement," *Nuclear Technology*, vol. 81, no. 1, pp. 100–113, 1988.

[19] R. O. Abdel Rahman, D. H. A. Zin El Abidin, and H. Abou-Shady, "Assessment of strontium immobilization in cement-bentonite matrices," *Chemical Engineering Journal*, vol. 228, pp. 772–780, 2013.

[20] R. O. Abdel Rahman and A. A. Zaki, "Assessment of the leaching characteristics of incineration ashes in cement matrix," *Chemical Engineering Journal*, vol. 155, no. 3, pp. 698–708, 2009.

[21] N. M. Sami, O. A. Moamen, M. I. El-Dessouky, and A. M. El-Kamash, "Assessment the leaching characteristics and long-term leaching behavior of some radionuclides from synthesized zeolite cement matrix," *Cement and Concrete Research*, vol. 143, Article ID 106357, 2021.

[22] X. Xu, H. F. Bi, Y. Yu et al., "Low leaching characteristics and encapsulation mechanism of Cs^{+} and Sr^{2+} from SAC matrix with radioactive IER," *Journal of Nuclear Materials*, vol. 544, Article ID 152701, 2021.

[23] Z. Zheng, Y. Li, H. Sun, Z. Zhang, and X. Ma, "Coupling effect of NaOH and $NaNO_3$ on the solidified fly ash-cement matrices containing Cs^{+}: reaction products, microstructure and leachability," *Journal of Nuclear Materials*, vol. 539, Article ID 152252, 2020.

[24] Z. Zheng, Y. Li, Z. Zhang, and X. Ma, "The impacts of sodium nitrate on hydration and microstructure of Portland cement and the leaching behavior of Sr^{2+}," *Journal of Hazardous Materials*, vol. 388, Article ID 121805, 2020.

[25] Z. Zheng, X. Ma, Z. Zhang, and Y. Li, "In-situ transition of amorphous gels to Na-P1 zeolite in geopolymer: mechanical and adsorption properties," *Construction and Building Materials*, vol. 202, pp. 851–860, 2019.

[26] S. Miyamoto, H. Minagawa, and M. Hisada, "Deterioration rate of hardened cement caused by high concentrated mixed acid attack," *Construction and Building Materials*, vol. 67, pp. 47–54, 2014.

[27] K. Kurumisawa, T. Nawa, H. Owada, and M. Shibata, "Deteriorated hardened cement paste structure analyzed by XPS and ^{29}Si NMR techniques," *Cement and Concrete Research*, vol. 52, pp. 190–195, 2013.

[28] Z. Zheng, Y. Li, J. Yang, M. Cui, H. Wang, and X. Ma, "Insights into the deterioration of C-S-H gels in hardened cement pastes with different $NaNO_3$ concentrations," *Construction and Building Materials*, vol. 259, Article ID 120423, 2020.

[29] T. Gutberlet, H. Hilbig, and R. E. Beddoe, "Acid attack on hydrated cement-Effect of mineral acids on the degradation process," *Cement and Concrete Research*, vol. 74, pp. 35–43, 2015.

[30] K. Wan, Y. Li, and W. Sun, "Experimental and modelling research of the accelerated calcium leaching of cement paste in ammonium nitrate solution," *Construction and Building Materials*, vol. 40, pp. 832–846, 2013.

[31] Z. Zheng, Z. Bao, J. Yang, M. Cui, X. Ma, and Y. Li, "The products transformation and leaching behavior in solidified cement matrices under the coupling actions of "water-heat-chemistry"," *Construction and Building Materials*, vol. 323, Article ID 126565, 2022.

[32] W. Kurdowski, "The protective layer and decalcification of CSH in the mechanism of chloride corrosion of cement paste," *Cement and Concrete Research*, vol. 34, no. 9, pp. 1555–1559, 2004.

[33] R. Abdelrahman, A. A. Zaki, and A. M. El-Kamash, "Modeling the long-term leaching behavior of ^{137}Cs, ^{60}Co, and $^{152,\ 154}Eu$ radionuclides from cement-clay matrices," *Journal of Hazardous Materials*, vol. 145, no. 3, pp. 372–380, 2007.

[34] A. El-Kamash, A. M. El-Dakroury, and H. F. Aly, "Leaching kinetics of ^{137}Cs and ^{60}Co radionuclides fixed in cement and cement-based materials," *Cement and Concrete Research*, vol. 32, no. 11, pp. 1797–1803, 2002.

[35] Q. Tian and K. Sasaki, "Application of fly ash-based materials for stabilization/solidification of cesium and strontium," *Environmental Science and Pollution Research*, vol. 26, no. 23, pp. 23542–23554, 2019.

[36] N. K. Lee, H. R. Khalid, and H. K. Lee, "Adsorption characteristics of cesium onto mesoporous geopolymers containing nano-crystalline zeolites," *Microporous and Mesoporous Materials*, vol. 242, pp. 238–244, 2017.

[37] J. Y. Jiang, P. Wang, and D. S. Hou, "The mechanism of cesium ions immobilization in the nanometer channel of calcium silicate hydrate: a molecular dynamics study," *Physical Chemistry Chemical Physics*, vol. 19, no. 41, pp. 27974–27986, 2017.

[38] N. D. Evans, "Binding mechanisms of radionuclides to cement," *Cement and Concrete Research*, vol. 38, no. 4, pp. 543–553, 2008.

[39] M. Youssef, R. J. M. Pellenq, and B. Yildiz, "Docking ^{90}Sr radionuclide in cement: an atomistic modeling study," *Physics and Chemistry of the Earth, Parts A/B/C*, vol. 70-71, pp. 39–44, 2014.

[40] J. Tits, E. Wieland, C. J. Muller, C. Landesman, and M. H. Bradbury, "Strontium binding by calcium silicate hydrates," *Journal of Colloid and Interface Science*, vol. 300, no. 1, pp. 78–87, 2006.

[41] T. Iwaida, S. Nagasaki, and S. Tanaka, "Sorption study of strontium onto hydrated cement phases using a sequential desorption method," *Radiochimica Acta*, vol. 88, no. 8, pp. 483–487, 2000.